Journal of Geodesy (2023) 97:20
https://doi.org/10.1007/s00190-023-01707-3

ORIGINAL ARTICLE

Estimating C_{30} coefficients for GRACE/GRACE-FO time-variable gravity field models using the GRACE-OBP approach

Yu Sun[1,2,3] · Yang Li[4,5] · Xiang Guo[6] · Jinyun Guo[7]

Received: 8 November 2021 / Accepted: 23 January 2023

Abstract

Recently, C_{30} coefficients of time-variable gravity field models from GRACE and GRACE-Follow On (GRACE/GRACE-FO) are reported to contain larger uncertainties when only one of the two onboard accelerometers is fully functional, which mainly concerns the GRACE-FO period and the final stage of the GRACE period. Using these problematic coefficients leads to incorrect mass change (rate) estimates, especially over Antarctic Ice-Sheet (AIS), and a replacement with those from satellite laser ranging (SLR) is currently recommended. In this study, we aim to discuss the possibility of improving the C_{30} coefficients by extending the GRACE-OBP approach that has previously been applied to the estimation of geocenter motion and variations in the Earth's dynamic oblateness. Such an approach mainly relies on GRACE/GRACE-FO level 2 products and an ocean bottom pressure model, and it produces compatible coefficients with the GRACE/GRACE-FO product labeled as GSM. With a numerical experiment, we demonstrate the effectiveness of the proposed approach and identify the optimal implementation parameter setup. The resulting C_{30} coefficient time series is generally consistent with those based on SLR and the original solutions from the GRACE dual-accelerometer period, but with differences in the annual amplitude estimates. Then, we obtain C_{30} coefficients based on real data and check the AIS mass change time series with and without replacing the original ones with our solution. Our C_{30} solution ensures consistent linear trend estimates for the dual- and single-accelerometer periods.

Keywords GRACE · GRACE-FO · C_{30} · Antarctic Ice-Sheet · Mass change · Satellite Laser Ranging

1 Introduction

The Gravity Recovery and Climate Experiment (GRACE) mission (Tapley et al. 2004), jointly sponsored by the National Aeronautics and Space Administration (NASA) and the German Aerospace Center (DLR), has been providing time-variable gravity (TVG) field models for more than 15 years (April 2002–June 2017). Thanks to the mission, we

✉ Xiang Guo
xiangguo@hust.edu.cn

Yu Sun
jade.yusun@outlook.com

Yang Li
isyang.li@outlook.com

Jinyun Guo
jinyunguo1@126.com

1 Key Lab of Spatial Data Mining and Information Sharing, Ministry of Education, Fuzhou University, Wulongjiang North Road, Fuzhou 350108, Fujian, China

2 National Engineering Research Center of Geospatial Information Technology, Fuzhou University, Wulongjiang North Road, Fuzhou 350108, Fujian, China

3 National & Local Joint Engineering Research Center of Satellite Geospatial Information Technology, Fuzhou University, Wulongjiang North Road, Fuzhou 350108, Fujian, China

4 State Key Laboratory of Geodesy and Earth's Dynamics, Innovation Academy for Precision Measurement Science and Technology, Chinese Academy of Sciences, Xudong Street, Wuhan 430077, Hubei, China

5 University of Chinese Academy of Sciences, Yanqihu East Road, Beijing 100049, China

6 MOE Key Laboratory of Fundamental Physical Quantities Measurement and Hubei Key Laboratory of Gravitation and Quantum Physics, PGMF and School of Physics, Huazhong University of Science and Technology, Luoyu Road, Wuhan 430074, Hubei, China

7 College of Geodesy and Geomatics, Shandong University of Science and Technology, Qianwangang Road, Qingdao 266000, Shandong, China

Published online: 02 March 2023

are now able to observe mass transportation in the Earth system directly at monthly intervals for a spatial resolution down to 300–500 km. Such measurements are unique and immensely useful in multiple research fields, including hydrology, geophysics and oceanography (Tapley et al. 2019). The valuable TVG records are being extended (at the same spatial–temporal resolution) since June 2018 thanks to the launch of the GRACE-Follow On (GRACE-FO) mission, which successfully ensures the data continuity before the next-generation gravity mission, e.g., GRACE-2, is available (Landerer et al. 2020). The resulting global monthly mass change is reported to have an equivalent precision with that from the GRACE (Landerer et al. 2020) which implies that the TVG models from GRACE and GRACE-FO are of the same quality. To achieve as accurate mass change estimates as possible, sophisticated post-processing procedures are still needed to suppress errors. Among others, the very low-degree coefficients need to be treated with special care. For example, changes in degree-1 coefficients (ΔC_{10}, ΔC_{11}, ΔS_{11}) do not exist in TVG models as both missions are insensitive to geocenter motions, which is defined as the relative movement between the center of mass of the earth system (CM) and the center of figure of the solid earth (CF) (e.g., Wu et al. 2012) (the symbol "Δ" will be dropped hereafter for simplicity, but all coefficients should be understood as time variations). As a result, external degree-1 solutions (TN-13, Sun et al. 2016b) should be added to the TVG models for completeness. Another well-known post-processing procedure is the replacement of the GRACE/GRACE-FO C_{20} coefficients with more reliable solutions (e.g., Cheng et al. 2011; Sun et al. 2016a, 2019) as the original ones are contaminated by unexpected large uncertainties due to reasons that are still not fully understood (Cheng and Ries 2017). Recently, original GRACE/GRACE-FO C_{30} coefficients since August 2016 are also reported to contain large uncertainties (Loomis et al. 2020). Except for August 2016, which is due to the relatively less data collected during that month, this can be attributed to the fact that only one of the two accelerometers is fully functional. For the final stage of the GRACE mission, the accelerometer on GRACE-B is shut down since November 2016 (note that none of the accelerometers are functional in September and October 2016 and in February and March 2017, hence no TVG models are available for those months; May 2017 is another exception as both accelerometers are functional) as an effort to extend the overall mission lifetime. Fortunately, an algorithm (Bandikova et al. 2019) has been developed to "transplant" the GRACE-A non-gravitational forces measurements onto GRACE-B to ensure the production of TVG models. For GRACE-FO, the accelerometer measurements on GRACE-D are not in use shortly after launch for notable higher noise level than the one on GRACE-C (Loomis et al. 2020). Therefore, a similar transplant approach has been applied for the GRACE-FO mission. Such a situation could last for the whole lifetime of GRACE-FO unless we can develop a more sophisticated algorithm making full use of the two accelerometers. Since the problematic time interval mainly concerns the single-accelerometer span, we do not distinguish between the period since August 2016 and the period when only one accelerometer is fully functional in this study.

Among others, using the corrupted C_{30} coefficients severely degrades the Antarctic Ice-Sheet (AIS) mass change (rate) estimates. As a result, it is recommended to replace the C_{30} coefficients with solutions of higher quality for the single-accelerometer span. One of the options is to use the solution based on Satellite Laser Ranging (SLR) data. Thanks to the Laser Relativity Satellite (LARES) launched in 2012, the quality of C_{30} coefficients is largely improved (by a factor of 8) compared to the solutions without including LARES data. However, LARES is currently the only SLR satellite sensitive to C_{30} coefficients due to a combination of the lowest area to mass ratio of all artificial satellites, unique inclination (69.5°) and relatively low altitude (1440 km) (e.g., Sośnica et al. 2015). More importantly, the strong correlation between C_{30} and C_{50} prevents a full recovery of their seasonal signals (Devoti et al. 2001; Sośnica et al. 2015). Currently, the SLR solutions are validated by comparisons with those from GRACE during the dual-accelerometer period. Unfortunately, there are still large differences between various SLR solutions (see Fig. S1 in the supplementary material).

Other than estimating low-degree coefficients directly from SLR data, it is also possible to obtain reasonable solutions from the GRACE-OBP approach. The method was first proposed by Swenson et al. (2008) in an effort to estimate geocenter motions by combining GRACE data and an ocean bottom pressure model (OBP). The theory is straightforward and can be easily extended to estimate other low-degree coefficients. Sun et al. (2016a) coestimated C_{20} coefficients which showed reasonable agreement with SLR solutions and the estimates based on the fingerprint approach (Sun et al. 2019). In addition, the authors improved the original method by using more realistic distribution of the water exchanged between land and ocean by taking into account self-attraction and loading (SAL) effects. Then, a numerical study (Sun et al. 2016b) further confirmed the effectiveness of the method and found the optimal implementing details such as the truncation degree of the input GRACE TVG models and the ocean function used to calculate the total ocean mass variations. In that study, the authors identified that considering SAL effects is critical to produce degree-1 and C_{20} coefficients with the correct annual variations and trends. They also conclude that the results are sensitive to the truncation degree and the signal leakage from land to ocean. The leaked signals are reduced by using an ocean function with a buffer zone about 200 km wide. Alternatively, it can be solved by applying a forward modeling technique (Chen et al. 2015; Jeon et al. 2018). Sun

et al. (2017) proposed a methodology framework that takes into account of both GRACE and OBP model error information. Such a method can be reduced to the GRACE-OBP approach provided that the oceanic data contain only white noise and the GRACE data are noise-free. Most recently, Seo et al. (2021) demonstrated that the GRACE-OBP approach is also capable of estimating changes in polar motion, i.e., the C_{21} and S_{21} coefficients.

In this study, we aim to explore the possibility of estimating the C_{30} coefficients through the GRACE-OBP approach described in Sun et al. (2016b). The result is valuable for mutual comparisons with existing solutions. More importantly, the approach provides C_{30} solutions dependent on the input TVG models. And we expect the GRACE/GRACE-FO post-processing procedure of replacing C_{30} coefficient is more reasonable to use dedicated C_{30} for each TVG models rather than the same solution from an independent technique considering the differences in various GRACE/GRACE-FO TVG models.

2 Methodology and input data

The derivation of the C_{30} coefficient mimics the way of deriving degree-1 and C_{20} as documented in Sun et al. (2016a). Different from SLR data processing, which normally requires simultaneous estimation of spherical harmonic coefficients up to a certain degree (e.g., 5) due to correlations between coefficients, the GRACE-OBP approach has the advantage that estimation of each coefficient is relatively independent. In other words, the method allows for focusing only on the interested coefficients, while other coefficients, such as C_{21}, S_{21}, C_{22}, S_{22}, which are beyond the scope of this study, can remain unchanged:

$$\begin{bmatrix} I_{10C}^{10C} & I_{11C}^{10C} & I_{11S}^{10C} & I_{20C}^{10C} & I_{30C}^{10C} \\ I_{10C}^{11C} & I_{11C}^{11C} & I_{11S}^{11C} & I_{20C}^{11C} & I_{30C}^{11C} \\ I_{10C}^{11S} & I_{11C}^{11S} & I_{11S}^{11S} & I_{20C}^{11S} & I_{30C}^{11S} \\ I_{10C}^{20C} & I_{11C}^{20C} & I_{11S}^{20C} & I_{20C}^{20C} & I_{30C}^{20C} \\ I_{10C}^{30C} & I_{11C}^{30C} & I_{11S}^{30C} & I_{20C}^{30C} & I_{30C}^{30C} \end{bmatrix} \begin{bmatrix} C_{10}^{m} \\ C_{11}^{m} \\ S_{11}^{m} \\ C_{20}^{m} \\ C_{30}^{m} \end{bmatrix} = \begin{bmatrix} C_{10}^{\text{ocean}} \\ C_{11}^{\text{ocean}} \\ S_{11}^{\text{ocean}} \\ C_{20}^{\text{ocean}} \\ C_{30}^{\text{ocean}} \end{bmatrix} - \begin{bmatrix} G_{10C} \\ G_{11C} \\ G_{11S} \\ G_{20C} \\ G_{30C} \end{bmatrix}, \tag{1}$$

where

$$I_{30C}^{11S} = \frac{1}{4\pi} \int \bar{P}_{11}(\cos\theta)\sin(1\times\phi)\vartheta(\theta,\phi)\,\bar{P}_{30}(\cos\theta)\cos(0\times\phi))d\Omega \quad \text{(similar for the other elements of matrix } I\text{)}, \tag{2}$$

and

$$G_{30C} = \frac{1}{4\pi} \int \bar{P}_{30}(\cos\theta)\cos(0\times\phi)\vartheta(\theta,\phi) \sum_{l=2}^{\infty}\sum_{m=0}^{l} \bar{P}_{30}(\cos\theta)\{C_{lm}^{m}\cos m\phi + S_{lm}^{m}\sin m\phi\}d\Omega \quad \text{(similar for the other elements of vector}G\text{)}. \tag{3}$$

in which the summations exclude the terms that are estimated, integrals are defined over the entire globe, $d\Omega = \sin\theta\, d\theta\, d\phi$ is an element of solid angle. Indices l and m represent the spherical harmonic degree and order, respectively. $\bar{P}_{lm}$ are normalized associated Legendre functions. θ is colatitude in spherical coordinates, ϕ is longitude, and $\vartheta(\theta,\phi)$ denotes the ocean function, which equals 1 over oceans and 0 over land. Here, the spherical harmonic coefficients C_{10}^{m}, C_{11}^{m}, S_{11}^{m}, C_{20}^{m}, C_{30}^{m}, C_{lm}^{m}, and S_{lm}^{m} are the mass coefficients describing the surface mass change. $C_{\text{lm}}^{\text{ocean}}$ are oceanic mass coefficients derived from an ocean model. Once the targeted low-degree coefficients are obtained, we can easily convert these coefficients to the dimensionless Stokes coefficients according to Wahr et al. (1998):

$$\begin{bmatrix} C_{\text{lm}} \\ S_{\text{lm}} \end{bmatrix} = \frac{a\rho_{\text{earth}}(2l+1)}{3(1+k_l)} \begin{bmatrix} C_{\text{lm}}^{m} \\ S_{\text{lm}}^{m} \end{bmatrix}, \tag{4}$$

where a denotes the average Earth radius, ρ_{earth} is the average density of the solid Earth, and k_l represents the gravitational elastic load Love number of degree l.

The input of equation (1) has already been discussed explicitly in previous studies (e.g., Swenson et al. 2008; Sun et al. 2016b). The oceanic input (e.g., C_{30}^{ocean}) is composed of two components: (1) the signals due to internal mass redistribution within oceans and (2) the signals due to ocean–land water exchange that varies the total ocean mass. When working with level 2 GRACE/GRACE-FO product (labeled as GSM coefficients), the oceanic signal of the Atmosphere and Ocean Dealiasing level 1B RL06 (AOD1B RL06) data needs to be subtracted from the oceanic input (Swenson et al. 2008). Consequently, the oceanic low-degree input contains only the signal caused by ocean–land water exchange, which is computed also based on the GSM coefficients with an iterative procedure in order to take into account the lack of the several coefficients to be estimated. As a result, the input data are practically limited only to the GRACE/GRACE-FO GSM coefficients in theory. In reality, this is not exactly the case because the derivation of the GRACE-OBP approach relies on the assumption that the mass change signals take places at the surface of the earth (Swenson et al. 2008). Any signals originate from the deep interior of the solid earth should be modeled and removed. So far, the detectable time-variable solid earth signals are primarily caused by the tectonic sig-

nals due to mega-thrust earthquakes and the glacial isostatic adjustment (GIA). The mass-change signals from large earthquakes are rather restricted to regional scales, and we do not attempt to model those signals following several previous studies (e.g., Swenson et al. 2008; Sun et al. 2016a). However, the GIA representing the ongoing earth's viscoelastic response to past glacial cycles is a process at global scale and their contributions to the estimation of C_{30}, restricted to the linear trend, have to be considered.

3 Numerical experiments

3.1 Simulation of input data

According to Sun et al. (2016b), the degree-1 and C_{20} solutions are largely dependent on the implementation parameters mentioned above. In this study, while including SAL effects is still necessary, the truncating degree and the choice of ocean function may vary for the optimization of five simultaneously estimated coefficients instead of four. Therefore, before we apply the method to real GRACE/GRACE-FO data, we have implemented a numerical study similar to that of Sun et al. (2016b) to verify the effectiveness of the method as well as to find the optimal setup of implementing parameters.

For the numerical study, we need to prepare realistic input GRACE/GRACE-FO TVG models in the form of GSM coefficients. This requires the construction of the error-free TVG models and sets of errors to mimic those in the actual GRACE/GRACE-FO TVG models. We first construct true synthetic earth model of surface mass changes by summing up the four components provided by the updated Earth System Model (ESM) (Dobslaw et al. 2015) including atmosphere (A), ocean (O), terrestrial water (H), and ice sheets (I). These components are based on advanced geophysical models and are provided in Stokes coefficients up to degree and order 180 (corresponding to a spatial resolution of about 100 km in terms of half wavelengths) with a temporal resolution of 6 h covering a 12-year period (1995–2006) (Dobslaw et al. 2015; Gruber et al. 2011). The updated ESM model assumes a uniform distribution of the ocean–land exchanging water over the oceans. We have improved it by taking into account SAL effects by solving the sea level equation. Since the TVG models do not contain atmospheric and oceanic signals modeled by the AOD1B product, we also need to remove an equivalent product from the true synthetic earth model. Fortunately, along with the earth system components, a product named DEAL is distributed for such a purpose. The DEAL product is essentially an atmospheric and oceanic dealiasing model equivalent to the error-free AOD1B RL06 product. It is different from the combination of A and O components as it omits mesoscale oceanic variabilities as well as the total ocean mass changes due to ocean–land water exchange, which are also ignored in the current AOD1B product. Therefore, the error-free TVG models are obtained by summing up the components A, O, H, I and subtracting the DEAL product (AOHI - DEAL). Then, we computed their monthly averages to match the GRACE/GRACE-FO TVG models' temporal resolution. Further, we identify the missing months in real GRACE solution for a 12-year period (2003–2014) and shift the time-tags backward by 8 years to match the ESM model period. These missing months are deliberately ignored in the synthetic TVG models to be more consistent with the real GRACE data.

To simulate random errors presented in the real TVG models, we need to consider two types of errors: (1) errors in the AOD1B product which enters the TVG models when subtracting the AOD1B product from the raw observation data and (2) errors originated from multiple contributing sources including uncertainties in onboard sensors and orbit determination, etc., that primarily manifest themselves as random north–south stripes in a global mass redistribution map. The first type of errors are already provided in the AOerr files distributed along with the DEAL product. Adding AOerr coefficients to the DEAL product will result in a realistically perturbed dealiasing model equivalent to the AOD1B product. The random stripe errors, on the other hand, need to be constructed by ourselves. In Sun et al. (2016b), the authors have generated those errors on the basis of error covariance matrices of the CSR RL05 GRACE solutions according to equation (6) of that study. The obtained errors, though having the same statistic characteristics, may be significantly different from the actual errors carried in the real TVG models (Wiese et al. 2011).

Another method takes the residual fields between the filtered and unfiltered TVG solutions as the random stripe error realizations. This method implies the assumption that the applied filters are adequate to remove the random stripe errors. We have attempted to construct the random stripe errors by subtracting the filtered fields with DDK1-8 filters (Kusche et al. 2009) from the original unfiltered ones. The DDK decorrelation filters use the error covariance matrices and an a priori signal covariance matrix in the spherical harmonic domain and ensure more aggressive damping for higher noise and/or lower signal level and vice versa. The effect of such filters is similar to that of a combination of Gaussian filtering (Wahr et al. 1998) and empirical destriping (Swenson and Wahr 2006). However, the simulated random stripe errors seem to underestimate the errors in the low degrees. This is expected as the filters are less effective on the lower degrees.

As a result, we decided to take the residual fields between different GRACE TVG solutions as the random stripe errors. We have collected 5 latest releases of TVG solutions including Center for Space Research RL06 (CSR), Helmholtz

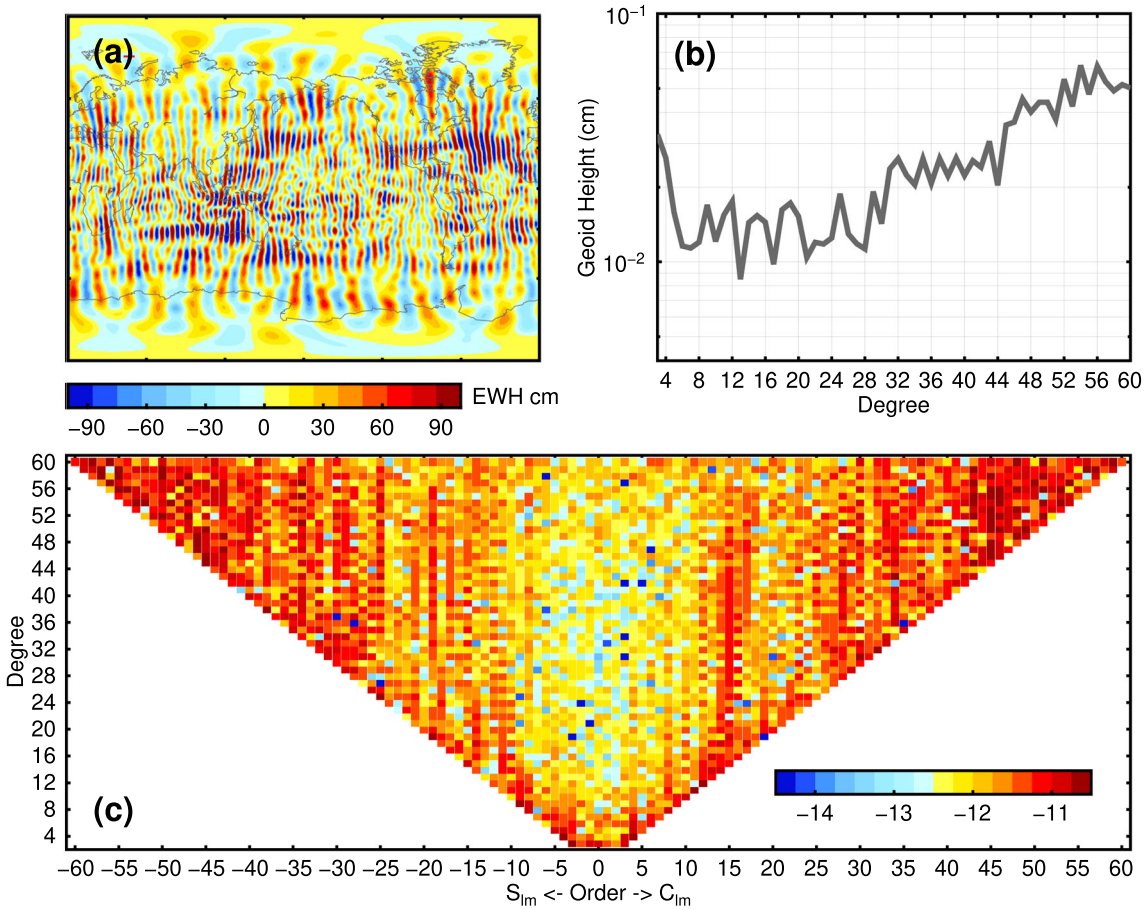

Fig. 1 Random stripe error realization by subtracting TVG model of GFZ from CSR for April 2002. We show its spatial distribution (**a**), geoid degree error (**b**), and logarithm of error in the spherical harmonic coefficients. Spherical harmonic coefficients lower than degree 3 are deliberately excluded

Centre Potsdam GFZ German Research Centre for Geosciences RL06 (GFZ), Jet Propulsion Laboratory RL06 (JPL), Institute of Geodesy at Graz University of Technology Release 2018 (ITSG) and International Combination Service for Time-variable Gravity Field (COST-G) (all accessed at http://icgem.gfz-potsdam.de/home). Here, we assume that all the 5 solutions are independent from each other (though the COST-G solution is essentially a weighted combination of various TVG solutions) and obtained altogether 10 sets of error realizations.

In Fig. 1, we present the simulated random stripe errors from the difference between CSR and GFZ models (CSR-GFZ, April 2002). Note that only spherical harmonic coefficients of degree 3 and above are shown as lower degrees that are not involved in our computation of the GRACE-OBP approach. In panel a, we show the spatial distribution of errors as mass change. The pronounced stripes are sufficiently representative for those in the original TVG models in terms of the magnitudes. In panel b-c, we show the geoid degree error and the logarithm of error in the spherical harmonic coefficients, respectively. Both of them are comparable to those shown in Wiese et al. (2011). Also, we have verified that other realizations of errors are similar (the case of CSR-COSTG is also shown in Fig. S2).

We have quantified the relative contributions of both types of errors to the five recovered coefficients. With a fixed implementation parameter setup (using a buffer width of 200 km and a truncation degree at 45, other setups result in very similar results), we consider the resulting time series of the five coefficients based on input GSM coefficients only subject to the errors provided by AOerr and those only subject to random stripe errors. Both results are then compared with those based on the error-free GSM coefficients. We find that the contribution of AOerr is less than 10 % of that due to the random stripe errors for all 5 coefficients. As a result, it is enough to consider the random stripe errors only.

Finally, we construct 10 sets of realistic TVG models by perturbing the error-free TVG models with the simulated errors. With the synthetic GRACE/GRACE-FO data, we estimate C_{30} coefficient based on various combinations of truncation degree and buffer width (the width of the buffer zone surrounding the continents that are deliberately inter-

preted as oceans). The tested truncation degrees range from 20 to 60. For each truncation degree, we test buffer width ranging from 50 to 400 km with a 50 km increment. For each particular combination of the two implementing parameters, we obtain the C_{30} time series based on all 10 sets of synthetic TVG models. For each C_{30} time series, we fit it with a regressing model including a bias, linear trend, annual and semiannual periodic terms.

In addition to the random errors, the OBP model may also contain non-negligible systematic errors, which will significantly affect the final results (Swenson et al. 2008). In this study, we will evaluate the OBP systematic errors by comparing two independent OBP models. Another thing worth noting is that we temporally ignored the solid earth component in the numerical experiments because it is very difficult to realistically simulate errors in the GIA models. Therefore, we also prefer to check their impacts by using different GIA models later when processing real data. However, the current numerical study should be sufficient for the purpose of selecting proper implementation parameters.

3.2 Selection of the optimal implementation parameters

In Fig. 2a–c, we show the annual amplitude, annual phase, and linear trend estimates of C_{30} time series from all 10 sets of synthetic TVG models based on all considered parameter combinations (only the 100 km, 150 km, 200 km, and 250 km cases are shown for clarity). The spreads of the results are indicated in each panel as light-colored bands and the solid lines shown inside (may not be in the middle) are the mean values. Clearly, when the buffer width for the ocean function is between 150 and 250 km, it is possible to recover the true amplitude by selecting suitable truncation degrees. There is a trade-off between the buffer width and the truncation degree. That is, wider buffers require lower truncation degrees to obtain closer annual amplitude to the true values (based on the original C_{30} coefficient time series of our error-free synthetic TVG models). For a 200 km buffer width, the truncation degree should be larger than 45, while for a 250 km buffer width, we can truncate the input TVG models around degree 30. The annual phase seems insensitive to the choice of implementation parameters, because all the combinations of buffer width and truncation degree allow estimating the true values within several days. The linear trend estimates, on the other hand, show an irregular behavior as the truncation degree increases. Taking the results using a 200 km wide buffer as an example, the values obtained are first rising and then drop as truncation degree increases.

Other than the C_{30} coefficient, we have also checked the implementation parameter setup for degree 1 and C_{20} (Fig. S2). All the considered coefficients show similar results as C_{30}. Therefore, it makes sense to select an overall optimal parameter setup for all five coefficients. Here, we compute quality indicators (QI) for the combination of annual variation (QI^{annual}) and linear trend (QI^{trend}) according to:

$$\begin{aligned} QI =& QI^{\text{annual}} + QI^{\text{trend}} \\ =& \sum_{\text{cf}=C_{10}}^{C_{30}} \sum_{i=1}^{n} \{(T_{\text{cf},i}^{\text{amp}} \sin(T_{\text{cf},i}^{\text{pha}}) - T_{\text{cf}}^{\text{amp}^{\text{t}}} \sin(T_{\text{cf}}^{\text{pha}^{t}}))^2 \\ &+ (T_{\text{cf},i}^{\text{amp}} \cos(T_{\text{cf},i}^{\text{pha}}) - T_{\text{cf}}^{\text{amp}^{t}} \cos(T_{\text{cf}}^{\text{pha}^{t}}))^2\} \\ &+ \sum_{\text{cf}=C_{10}}^{C_{30}} \sum_{i=1}^{n} (T_{\text{cf},i}^{\text{trend}} - T_{\text{cf}}^{\text{trend}^{t}})^2. \end{aligned} \tag{5}$$

where T_{cf} represents the time series of coefficient cf, which loops over the five estimated coefficients (scaled to describe mass changes in terms of equivalent water thickness). Subscript i means that the result is based on the ith realization of input GSM coefficients; n is the number of simulated GSM solutions, which is equal to 10. Superscripts amp, pha, trend, and rms stand for the annual amplitude, annual phase, and linear trend estimates of the corresponding time series, respectively; those with a superscript t refer to the synthetic truth.

Finally, as have been observed in Fig. 2d, several combinations of buffer width and truncation degrees give overall desirable results for the five coefficients. As a result, we decided to select the combination using a buffer width of 200 km and a truncation at degree 45 (denoted as BUF200 L45 hereafter). This parameter setup is also recommended in the study by Sun et al. (2016b), which is meant for the optimization of annual and linear trend signals in degree-1 and C_{20} coefficients. We have verified that the estimation of C_{30} has a negligible impact on the estimation of the degree-1 and C_{20} coefficients (Fig. 3).

For a more intuitive comparison, we directly compare the estimated C_{30} time series against the synthetic truth. In Fig. 4a, we plot the resulting C_{30} time series based on the 10 realizations of TVG models. We show the average C_{30} solution to aid an easier visual comparison with the synthetic true C_{30} time series. In addition, we have shown the residuals in Fig. 4b. The residuals are about an order of magnitude smaller, which suggests that the GRACE-OBP approach is able to estimate the C_{30} coefficients reasonably well using the selected implementation parameters. In addition, we have conducted a spectral analysis (Fig. 4c) on the synthetic true C_{30} coefficient time series and our estimates based on the optimal parameter setup. Clearly, all the periodic terms have been perfectly recovered.

4 Results based on real GRACE/GRACE-FO data

In this section, we compute C_{30} coefficients based on real GRACE/GRACE-FO RL06 solutions truncated at degree 60

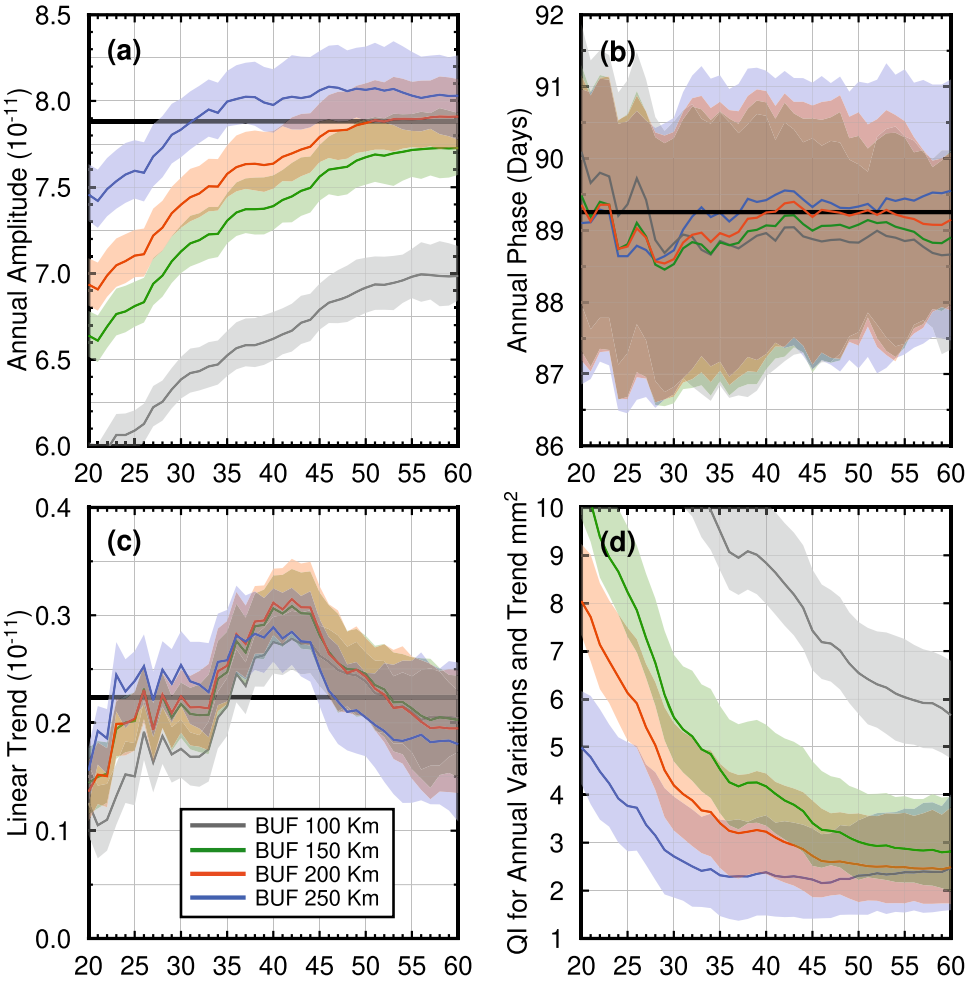

Fig. 2 Annual amplitude (**a**), phase (**b**), linear trend (**c**), and quality indicator (**d**) of the estimated C_{30} from 10 sets of synthetic TVG models. The solid lines represent the mean values, while the color bands indicate the actual spread of the 10 estimates. The true annual amplitude, phase, and linear trend are marked in corresponding panels (**a**–**c**) as black horizontal lines

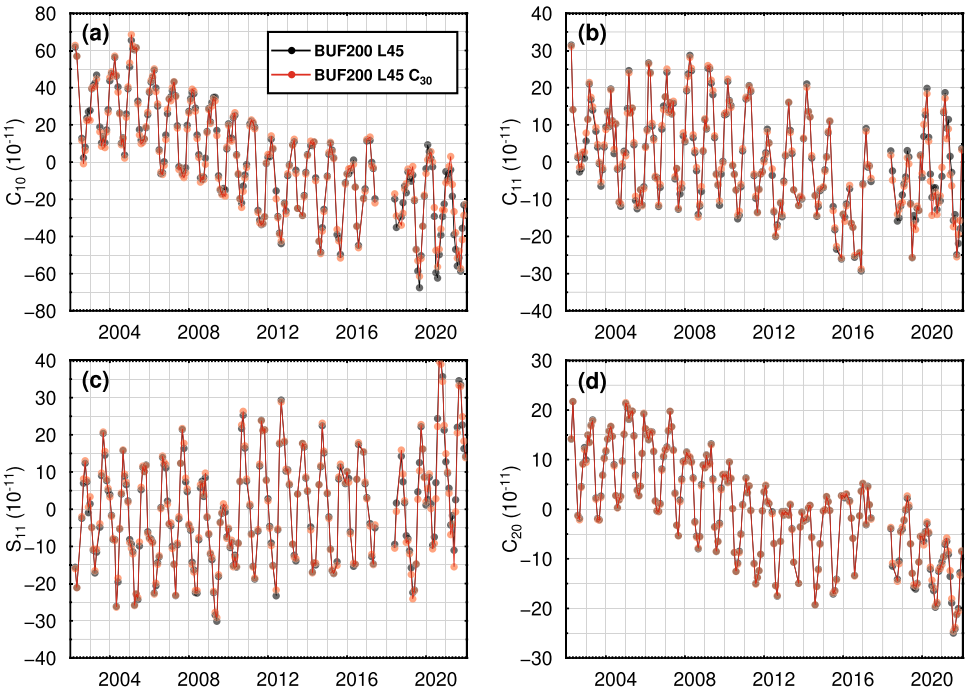

Fig. 3 Degree-1 and C_{20} coefficient estimated from the GRACE-OBP approach with and without estimating C_{30} coefficient

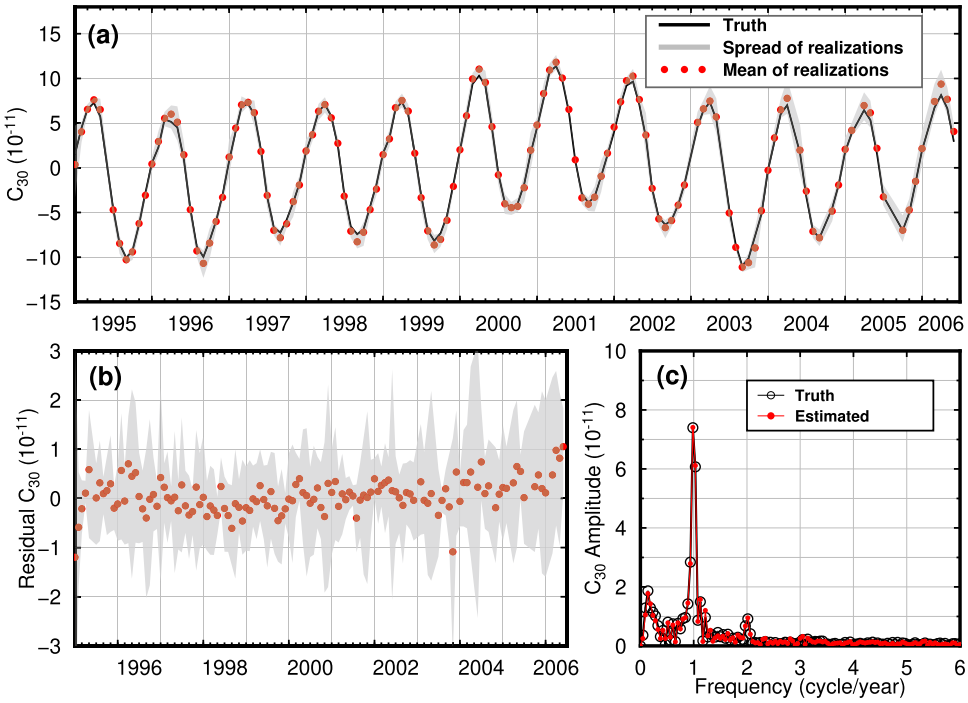

Fig. 4 A comparison of estimated C_{30} from 10 realizations of TVG models and the synthetic true C_{30} (**a**) and their residuals (**b**). The spread of the 10 realizations is shown as gray bands and their means are plotted as red dots. In panel **c**, we show the spectral analysis of the synthetic truth and the estimated C_{30} coefficient time series using the selected implementation parameter setup

from 3 data centers, namely CSR, GFZ, and JPL. Instead of directly computing the C_{30} coefficient time series based on the selected parameter setup from the numerical experiments, we repeat the same experiment shown in Fig. 2a–c to see how the annual signal and linear trend estimates change with the truncation degree and buffer width when the real data are applied. For the time being, we assume that the time-variable solid earth signals are adequately modeled by a GIA model provided by Peltier et al. (2018) (Peltier18). In Fig. 5, the annual signal and linear trend estimates are based on the solution for the period from January 2003 to June 2014 for a more consistent comparison with the synthetic case as the TVG models of the same period have been used to construct the random stripe errors. However, we have verified that the findings hold true for various time spans including the one covering the whole dual-accelerometer stage (April 2002–July 2016) and the one covering the whole available GRACE/GRACE-FO period (April 2002–August 2022).

The annual periodic signal statistics changes quite similarly as in the numerical experiments (Fig. 5a–b). As for the linear trend estimates, a similar effect of changing the implementation parameters is also found (Fig. 5 c), though the impact of the buffer width is slightly larger in the real data case. This might be partially attributed to the exclusion of GIA signals in the synthetic experiments. The general consistency of the results based on synthetic and real data

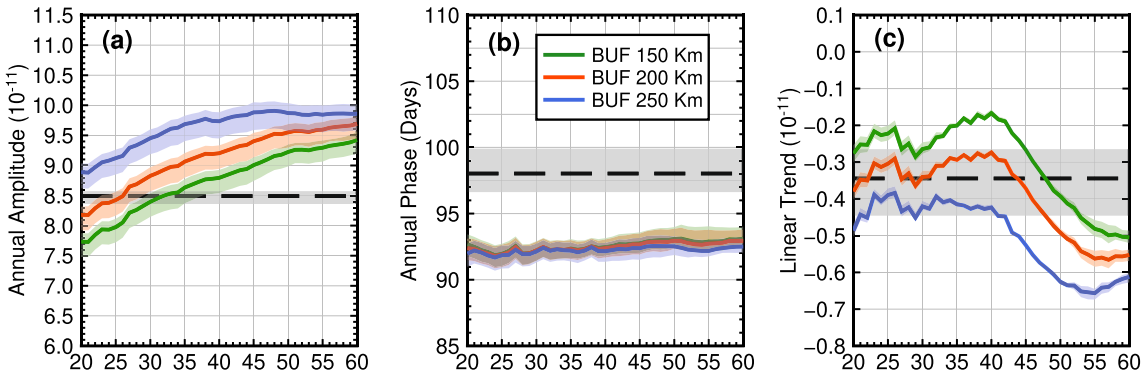

Fig. 5 Annual amplitude (**a**), annual phase (**b**), and linear trend (**c**) of the estimated C_{30} coefficient time series for real GRACE/GRACE-FO data processing (January 2003–June 2014). The solid lines represent the mean of the estimates based on CSR, GFZ, and JPL; the color bands stand for the actual spread of the estimates. The mean estimates and spreads of the original C_{30} from three data centers are shown as dashed black horizontal lines and color bands, respectively

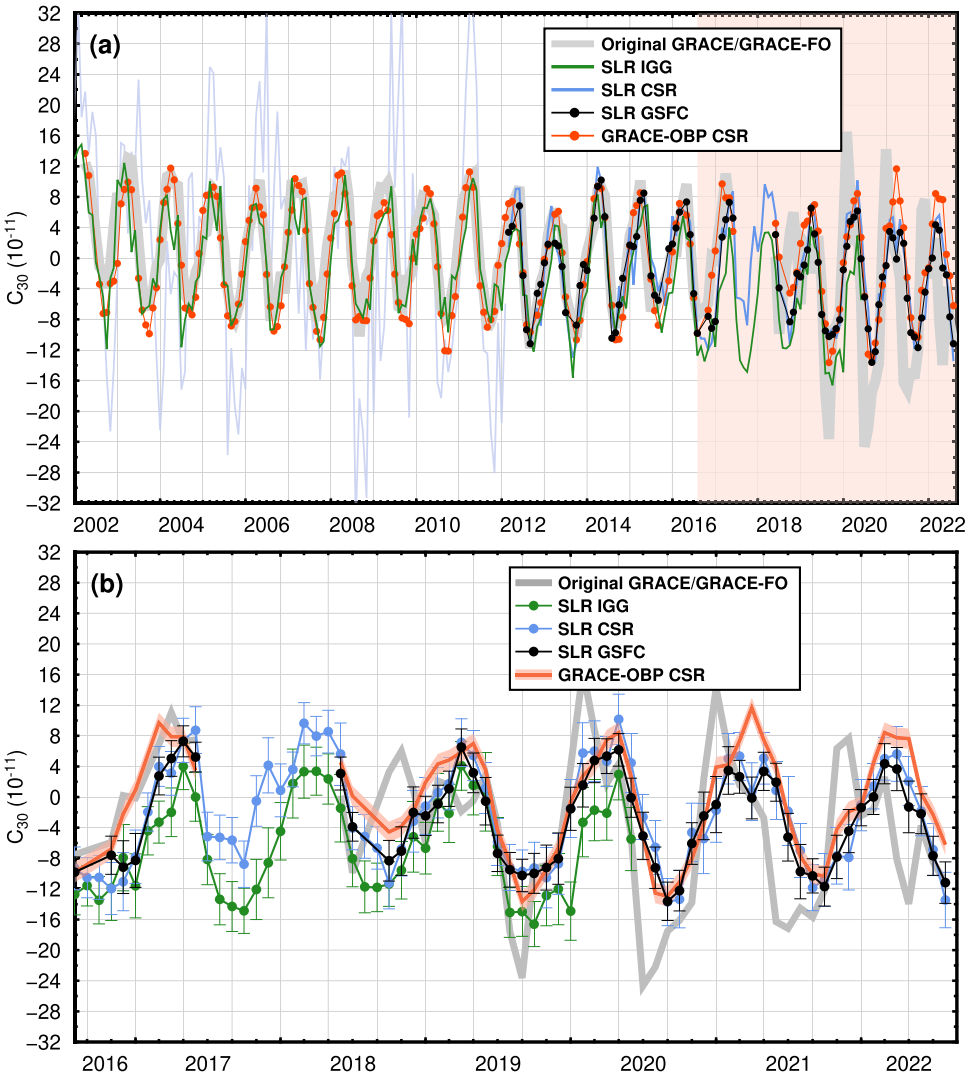

Fig. 6 A comparison of the original GRACE C_{30} coefficient time series (thick gray curve) and alternative solutions from GRACE-OBP approach and based on SLR data. We show the comparison of the whole period from April 2002 to August 2022 (**a**) and zoom in on the single-accelerometer period when the GRACE/GRACE-FO C_{30} coefficients need replacements (**b**). The single-accelerometer period is indicated in panel a with light red color. The biases in all time series are adjusted for the time span from April 2002 to August 2022

suggests that the recommended implementation parameter setup (BUF200 L45) is also valid in the real data processing.

Because the original C_{30} time series during the dual-accelerometer span has not been reported to have a problem so far, we have additionally shown their statistics (black dashed horizontal lines in all panels) as references. When using the selected implementation parameters, the annual amplitude is amplified from about 8.5×10^{-11} for the original GRACE solutions to about 9.5×10^{-11} for the GRACE-OBP ones. The annual phase estimates, on the other hand, only show a small offset (less than a week) between them. The linear trend estimates are not meaningful to discuss at this point as we have only used one GIA model without considering its uncertainties.

In Fig. 6, we show our C_{30} coefficient time series based on the preferred implementation parameter setup and compare it to original GRACE/GRACE-FO C_{30} time series as well as several solutions based on SLR data processing. To have a more clear sense of the differences among the C_{30} solutions, we zoom in on the recommended replacing period for a closer look (Fig. 6b). The uncertainties (1σ) are also shown either as error bars or as color bands. Note that the uncertainties in our time series are calculated based on the approach proposed by Ditmar et al. (2018).

In the figure, we have only shown the CSR solution for the sake of clarity. However, we have archived the key signal statistics including annual and semiannual amplitude and phase for the three TVG models for a more comprehensive comparison (Table 1). For the original GRACE/GRACE-FO solution, it is the large differences with respect to previous periods since August 2016 that triggers the concern on C_{30} coefficient's quality. Taking the result based on CSR TVG models as an example, the RMS of the time series is about 6.5×10^{-11} for the dual-accelerometer span, but jumps to 10.4×10^{-11} (increased by about 60 %) for the single-accelerometer portion of the time series. The annual variations of these two periods also show clear differences, $(8.3 \pm 0.2) \times 10^{-11}$ for the dual-accelerometer span com-

Table 1 Statistics of C_{30} time series for different time spans

Approach	RMS	Annual		Semiannual		Time span
	(10^{-11})	Amplitude (10^{-11})	Phase (Days)	Amplitude (10^{-11})	Phase (Days)	Year-month
ORI GRACE CSR	6.5	8.3 ± 0.2	98 ± 2	1.5 ± 0.2	294 ± 9	Dual-accelerometer period
ORI GRACE GFZ	6.5	8.2 ± 0.2	103 ± 2	1.5 ± 0.2	296 ± 10	2002.04–2016.07
ORI GRACE JPL	6.4	8.0 ± 0.2	98 ± 2	1.4 ± 0.2	306 ± 9	
GRACE-OBP CSR	7.0	9.5 ± 0.2	95 ± 1	0.7 ± 0.2	288 ± 14	
GRACE-OBP GFZ	6.7	9.1 ± 0.2	94 ± 1	0.6 ± 0.6	282 ± 18	
GRACE-OBP JPL	7.0	9.5 ± 0.2	94 ± 1	0.7 ± 0.2	291 ± 14	
GRACE-OBP CSR ECCO	7.0	9.4 ± 0.2	102 ± 1	0.8 ± 0.2	315 ± 17	
ORI GRACE CSR	10.4	10.4 ± 1.4	60 ± 7	2.8 ± 1.3	289 ± 27	Single-accelerometer period
ORI GRACE GFZ	9.3	9.6 ± 1.1	61 ± 7	1.7 ± 1.1	294 ± 38	2016.08–2022.08
ORI GRACE JPL	9.6	9.4 ± 1.2	55 ± 7	3.5 ± 1.2	311 ± 20	
GRACE-OBP CSR	7.0	9.6 ± 0.4	95 ± 2	1.9 ± 0.4	297 ± 12	
GRACE-OBP GFZ	6.4	8.8 ± 0.5	93 ± 3	1.9 ± 0.4	302 ± 14	
GRACE-OBP JPL	7.0	9.7 ± 0.4	95 ± 2	1.8 ± 0.4	297 ± 12	
ORI GRACE CSR	6.2	8.3 ± 0.6	100 ± 4	1.9 ± 0.5	297 ± 16	2012.03–2016.07
ORI GRACE GFZ	5.7	7.5 ± 0.5	105 ± 4	1.7 ± 0.5	299 ± 17	
ORI GRACE JPL	5.8	7.7 ± 0.6	100 ± 4	1.4 ± 0.6	313 ± 22	
GRACE-OBP CSR	6.5	9.3 ± 0.3	97 ± 2	0.5 ± 0.3	281 ± 33	
GRACE-OBP GFZ	6.2	8.8 ± 0.4	95 ± 2	0.4 ± 0.4	290 ± 52	
GRACE-OBP JPL	6.7	9.6 ± 0.3	96 ± 2	0.5 ± 0.3	299 ± 40	
SLR CSR	6.4	7.5 ± 0.6	100 ± 5	1.6 ± 0.6	290 ± 22	
SLR GSFC	5.7	7.1 ± 0.5	90 ± 4	2.4 ± 0.5	283 ± 12	
SLR IGG	6.2	7.6 ± 0.4	110 ± 3	1.5 ± 0.4	282 ± 16	

pared to $(10.4 \pm 1.4) \times 10^{-11}$ for the single-accelerometer span. Moreover, the mean annual phase estimates altered by more than a month from 98 ± 2 days to 60 ± 7 days. Such a problem, however, is not found in our solution. The RMS and annual variation estimates are quite consistent before and after August 2016, which suggests our solution successfully avoids the large uncertainties during the single-accelerometer period. For solutions of the other two centers, though statistic values vary, the general findings remain the same (Table 1).

Since SLR solutions are currently the recommended replacement of the problematic C_{30} coefficients, we are motivated to compare our solutions also with available SLR C_{30} time series. One of the SLR solutions (SLR CSR) is provided by CSR following Cheng et al. (2011), who estimates TVG models complete to degree 5 (plus C_{61} and S_{61}) by combining data from multiple SLR satellites. The noisy curve before 2012 clearly indicates the critical role of LARES in terms of determining C_{30}. The NASA's Goddard Space Flight Center (GSFC) SLR solution (SLR GSFC) is taken from TN-14 available at https://podaac.jpl.nasa.gov (Loomis et al. 2020). Since the time series is meant to be used for problematic GRACE/GRACE-FO C_{30} replacement, only solutions after the launch of LARES are provided. Also, months where GRACE/GRACE-FO solutions are missing are excluded intentionally. The third solution (SLR IGG) is provided by the Institute of Geodesy and Geoinformation (IGG) of University Bonn. In contrast to the other two SLR solutions, SLR IGG does not contain any LARES data. Instead, it applies a novel approach in which the leading empirical orthogonal functions derived from the GRACE TVG models are used to stabilize the SLR estimates to achieve desirable gravity field solutions with a high spatial resolution (complete to degree 60) dating back to 1992 (Löcher and Kusche 2020).

For a comparison with both the original GRACE and the SLR solutions, we have shortened the considered period to 4.5 years from March 2012 to July 2016 to avoid the problematic periods either for GRACE/GRACE-FO or for SLR. During such a period, all solutions visually agree well with each other and the RMSs of solutions are comparable (between 5.7×10^{-11} and 6.7×10^{-11}). However, the annual amplitude estimates of the GRACE-OBP approach are consistently larger than those of the original GRACE solutions and the SLR ones.

To further investigate such differences, we have additionally estimated the periodic signals in these time series through a spectral analysis. In Fig. 7a–c, we show the results

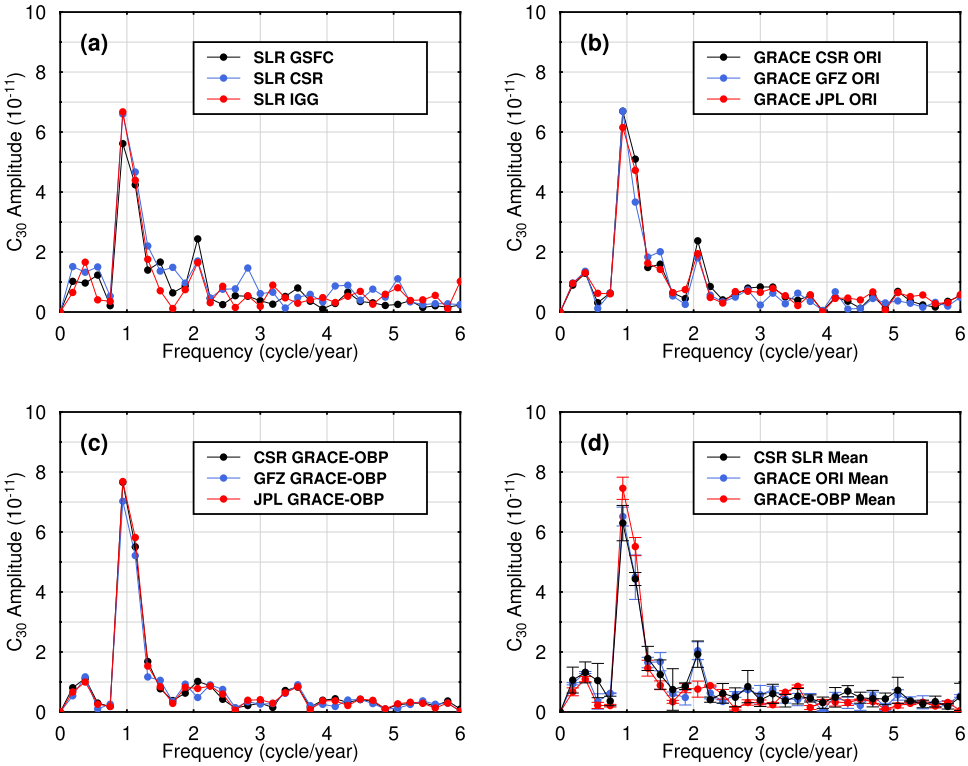

Fig. 7 Spectral analysis of C_{30} coefficient time series based on SLR data processing (**a**), GRACE (**b**), and GRACE-OBP approach (**c**). In panel **d**, we compare the results based on the three techniques with their standard deviations shown as error bars

Table 2 Linear trend estimates in C_{30} time series using different GIA models

Approach	Surface ($10^{-11}yr^{-1}$)	GIA ($10^{-11}yr^{-11}$)	Full ($10^{-11}yr^{-11}$)	Time span
Peltier18	-0.32 ± 0.02	0.19	-0.13 ± 0.02	2002.04–2022.08
A12	0.01 ± 0.02	-0.03	-0.02 ± 0.02	
Caron17	-0.44 ± 0.02	0.38	-0.06 ± 0.02	
SLR CSR	–	–	-0.08 ± 0.10	2012.03–2022.08
SLR GSFC	–	–	-0.26 ± 0.08	2012.03–2022.08
SLR IGG	–	–	-0.53 ± 0.11	2002.04–2020.06

for C_{30} coefficient time series based on SLR, GRACE, and GRACE-OBP, respectively. Each of the panels contains three solutions. And in panel d we show the averaged results from the above three techniques with error bars indicating the standard deviations. Note that amplitude results based on the spectral analysis are different from those estimated from least squares that are given in Table 1. For example, the annual amplitudes for all solutions are consistently smaller in spectral analysis. However, the estimates based on the GRACE-OBP approach are still larger than the other two techniques. This is probably due to the trade-off between the annual and semiannual amplitude estimates, where a larger annual amplitude is corresponding to a smaller semiannual component. In panel d, it is clear that the GRACE-OBP solution shows no significantly semiannual variations comparable to other C_{30} coefficient time series (Table 1). Since the GRACE-OBP approach is able to recover all periodic signals (Fig. 4c), in-depth investigations are needed to understand these differences.

Until now, we have only considered one GIA model (Peltier18) for the removal of the solid earth signals, which implies an unrealistic assumption that the GIA models are free of errors. Unfortunately, current GIA models carry uncertainties of unknown magnitude that may significantly affect the linear trend estimates in the C_{30} coefficient time series. GIA models covering all possible combinations of the elastic lithosphere thickness as well as the upper and lower mantle viscosity values need to be considered for a comprehensive evaluation, which is beyond the scope of this study. Here, we limited ourselves to compute the results by additionally applying two popular GIA models: A12 provided by A et al. (2012) and Caron17 from Caron et al. (2017).

In Table 2, we show the linear trend estimates for the whole GRACE/GRACE-FO period from April 2002 to August

2022. Because using different TVG models only causes negligible discrepancies (no greater than $0.03 \pm 10^{-11} yr^{-1}$), we only show the results based on CSR solutions. As can be seen, both the surface mass and the GIA-induced C_{30} trend show quite different estimates; we have only listed the results based on CSR TVG models. The differences between the estimates are as large as $0.4 \pm 10^{-11} yr^{-1}$ (using A12 and Caron17) for both surface mass and GIA-induced linear trends. However, when looking at the full trend, the linear trends from the two contributors are somehow neutralized. The differences are only at about $0.1 \pm 10^{-11} yr^{-1}$. This is expected because the surface mass-induced linear trend is dependent on the applied GIA model. We have also listed the linear trend estimates for three SLR C_{30} solutions, which show larger differences (about $0.3 \pm 10^{-11} yr^{-11}$). These values estimated for different time spans may not be directly compared with the GRACE-OBP results. However, the large differences suggest that the uncertainties caused by using the different GIA models are smaller than those in SLR data processing.

5 Impact of systematic errors in the OBP model

According to equation (1), the GRACE-OBP approach assumes that the oceanic low-degree coefficients are accurately known. This is also the underlying assumption of our study until now. Unfortunately, such information is still relying on the OBP predictions of the AOD1B RL06 product, which are provided in the GAD coefficients and distributed along with the GRACE level 2 data. We have only verified through the AOerr files that the random errors are negligible compared to those contained in the GSM coefficients. However, those coefficients may be also subject to non-negligible systematic errors which will alias into the final C_{30} estimates. In this study, we check if there are large systematic errors by comparing the OBP predictions of the AOD1B RL06 product to another OBP model from the Circulation and Climate of the Ocean version 4 release 4b (ECCO V4r4b) (Consortium et al. 2020). The AOD1B RL06 OBP is from the Max Planck Institute Ocean Model (MPIOM) (Jungclaus et al. 2013) and is forced with the European Centre for Medium-Range Weather Forecasts (ECMWF) atmospheric data. The ECCO OBP, on the other hand, is a data-assimilating model by fitting Massachusetts Institute of Technology general circulation model (MITgcm) (Marshall et al. 1997) to satellite and in situ data using weighted least squares minimization and forced with the re-analyzed atmospheric data ERA-Interim (Dee et al. 2011). We assume that the two OBP models are independent since they are based on different geophysical models and processing procedures. The ECCO OBP model is accessed as grids covering the oceans of the entire globe at a spatial resolution of 0.5 degree and a temporal resolution of a month. Then we expanded the ECCO OBP in the spherical harmonic domain to degree 100 in order to be consistent with the AOD1B RL06 product.

Systematic errors in the applied OBP model will affect the C_{30} coefficient estimates in two ways. First, systematic errors in the oceanic C_{30} coefficient derived from an OBP model will directly affect the resulting GSM C_{30} coefficient. Based on an analytical error propagation using equation (1), a 1 mm error in the oceanic C_{30} coefficient will be amplified by the inverse I matrix to about 2.4 mm in the C_{30} coefficient. The amplification factors are about 2.9, 1.1, 1.6, and 2.2 for C_{10}^{ocean}, C_{11}^{ocean}, S_{11}^{ocean}, and C_{20}^{ocean}, respectively. We directly compare the C_{30} coefficients of the two OBP models (Fig. 8a). Clearly, the C_{30}^{ocean} coefficients from the two OBP models are close and no evident systematic errors are observed. Second, systematic errors in the residual OBP field left in the GSM coefficients will also affect the estimation of C_{30}. Therefore, we further repeat the calculation of C_{30} coefficients by replacing OBP model from the GAD with that from the ECCO (by restoring GAD coefficients to the GSM coefficients and then remove the ECCO OBP coefficients). We show the resulting C_{30} time series agree very well in terms of RMS of the time series and annual amplitude. The annual phase estimates only differ by about 10 days (Fig. 8b, Table 1). Therefore, we conclude that there are likely no large systematic errors in the low-degree oceanic coefficients predicted by the current OBP models that will significantly affect the C_{30} coefficient estimation.

6 AIS mass change estimates

C_{30} coefficient plays an important role in calculating mass change (rate) at the Earth's surface, and the estimation of AIS mass change (rate) is one of the most relevant (Loomis et al. 2020). Here, we estimate AIS mass change using exactly the same post-processing techniques and the same input TVG models except for C_{30}. Specifically, we use the CSR RL06 TVG models complete to degree 60, destriped according to Duan et al. (2009), an improved version of the method proposed by Swenson and Wahr (2006). The resulting TVG models are filtered with a 300 km Gaussian smoother (Wahr et al. 1998) to suppress remaining stripes. We further applied a 300 km buffer zone to reduce the signal leakage to oceans. Degree-1 and C_{20} coefficients are taken from TN-13 and TN-14, respectively, so that the differences between the considered time series are solely due to the use of C_{30} coefficients from different sources. The A12 GIA model is applied to remove the secular solid Earth signal. We have verified that the above procedure produces an AIS mass change time series very close to those derived from the JPL Mascon solution. In Fig. 9, we plot five time series of the AIS mass

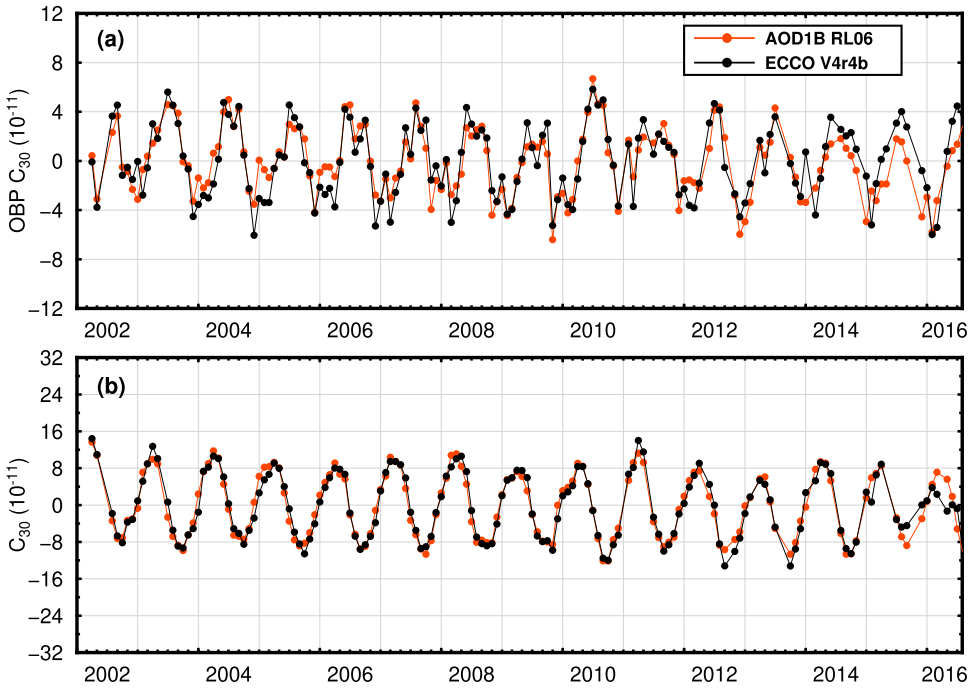

Fig. 8 Oceanic C_{30} coefficient from the AOD1B RL06 and ECCO V4r4b (**a**) OBP and the resulting C_{30} coefficient time series based on the two OBP models (**b**)

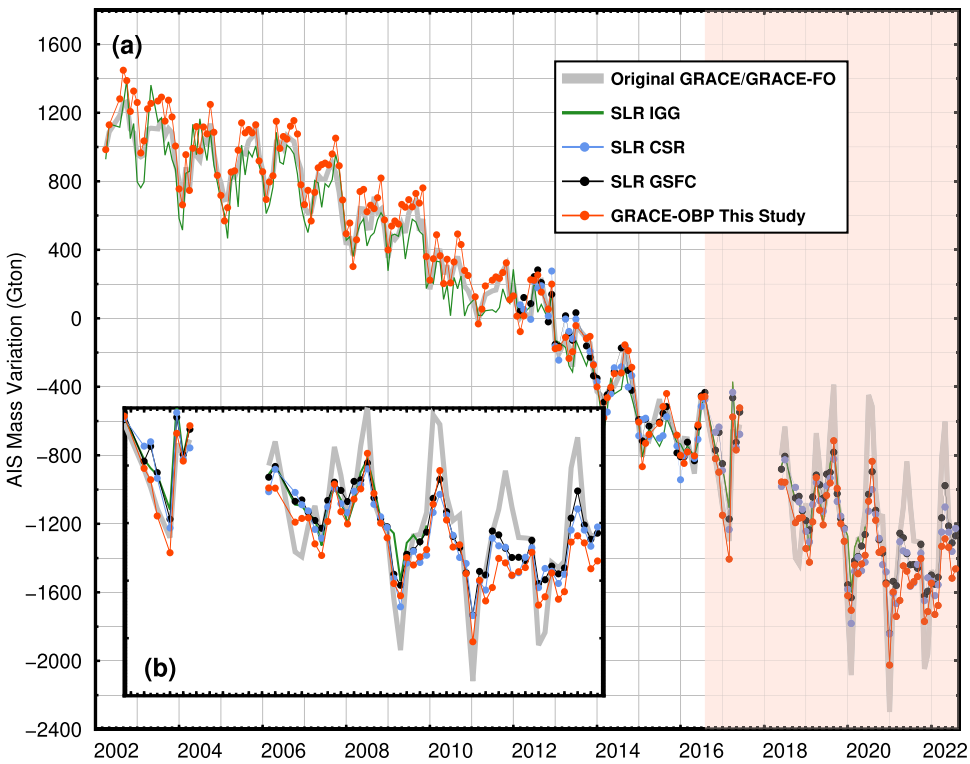

Fig. 9 AIS mass change estimated with and without replacing the C_{30} coefficient. The single-accelerometer period is indicated in panel **a** with light red color and enlarged in panel **b** for clarity

change time series using the C_{30} coefficients from the original GRACE/GRACE-FO TVG models, the GRACE-OBP approach and SLR data processing.

We first compare the five time series between March 2012 and July 2016 when reasonable estimates are available for all C_{30} solutions. Visually, all time series agree well with each other, their linear trends are quite close, and the largest difference is less than 20 Gt yr^{-1}, which is well within the model fit uncertainty (2σ). While the annual phase estimates are also practically equivalent, the annual amplitude of the time series using GRACE-OBP C_{30} shows significantly larger estimates compared to the one using original or SLR-based C_{30} coeffi-

Table 3 Trends and annual variations in Antarctica mass change time series

Approach	Trend	Annual		Time span
		Amplitude	Phase	
	(Gt yr^{-1})	(Gt yr^{-1})	(Days)	Year-month
ORI GRACE CSR	-154 ± 4	129 ± 14	249 ± 6	2007.01–2016.07
GRACE-OBP	-164 ± 4	159 ± 15	252 ± 5	
SLR GSFC	-150 ± 4	124 ± 14	239 ± 6	
SLR CSR	-173 ± 14	148 ± 47	280 ± 18	
SLR IGG	-157 ± 5	81 ± 17	263 ± 33	
ORI GRACE CSR	-125 ± 30	371 ± 52	196 ± 9	2016.08–2022.08
GRACE-OBP	-164 ± 19	229 ± 33	217 ± 9	
SLR GSFC	-172 ± 16	198 ± 28	205 ± 9	
SLR CSR	-183 ± 17	184 ± 30	218 ± 10	
SLR IGG	-164 ± 35	192 ± 39	221 ± 12	2016.08–2020.06
ORI GRACE CSR	-227 ± 13	160 ± 20	253 ± 7	2012.03–2016.07
GRACE-OBP	-233 ± 13	193 ± 20	252 ± 6	
SLR GSFC	-238 ± 12	152 ± 19	237 ± 7	
SLR CSR	-244 ± 16	142 ± 25	253 ± 10	
SLR IGG	-240 ± 13	107 ± 20	268 ± 11	
ORI GRACE CSR	-154 ± 4	200 ± 25	215 ± 7	2007.01–2022.08
GRACE-OBP	-169 ± 3	179 ± 16	236 ± 5	
SLR GSFC	-154 ± 2	147 ± 15	233 ± 6	
SLR CSR	-168 ± 5	141 ± 32	254 ± 13	
SLR IGG	-154 ± 3	98 ± 17	247 ± 10	2007.01–2020.06

cients (about 50 Gt). This is expected as our C_{30} time series has larger annual signals than other solutions.

In order to check the consistency of the linear trend before and after August 2016, we have estimated the linear trend for the time interval from January 2007 to July 2016. (The pre-2007 time series is excluded due to a significant change in the trend.) For the GSFC and CSR SLR-based time series, we simply assume that the estimates before March 2012 are exactly the same as the one based on the original solution. The estimates agree within the model fit uncertainty (2σ). For the period after July 2016, we have a relatively short time series (about 4 years), which may result in unstable trend estimates that are characterized by larger formal uncertainties. This is especially true when using the original GRACE C_{30} coefficients. The uncertainty 2σ of the linear trend estimates is about 126 Gt yr^{-1}, which is almost the same magnitude as the signal estimate itself.

When replacing the original C_{30} coefficients with those based on SLR, we observe relatively better consistency in the linear trend. However, the most consistent linear trend estimate is achieved when using the GRACE-OBP C_{30} coefficients (-164 ± 4 Gt yr^{-1} and -164 ± 19 Gt yr^{-1} for the dual- and single-accelerometer periods, respectively).

Annual amplitude estimates for the two periods, on the other hand, are not consistent no matter which C_{30} solution is in use. For the time series using the original C_{30} coefficients, the annual amplitude elevated from 129 ± 14 Gt to 371 ± 52 Gt, which is unreasonable. After the replacement with SLR or GRACE-OBP C_{30} solutions, we still obtain larger, though less dramatic, annual amplitude estimates.

7 Discussion and conclusions

In this study, we have extended the GRACE-OBP approach to coestimate C_{30} coefficients with degree-1 and C_{20} coefficients. The effectiveness of such a method has been validated and the optimal implementation parameter setup is selected through a numerical experiment, in which the random errors in the input data are realistically simulated. When processing real data, the variation of the linear trend and annual signal estimates according to the combinations of implementation parameters show similar behavior as in the numerical experiment, which allows us to conclude that the parameter setup identified from the numerical experiments is also suitable when applying to the real data. We have further confirmed that there are likely no significant systematic errors in the current OBP models from the AOD1B and ECCO. Also, the current GIA model seems to play a minor role in the uncertainties of the linear trend. As a result, we conclude that the GRACE-OBP approach is capable of estimating C_{30} coefficients. When estimating the AIS mass change, using our C_{30}

coefficients leads to the most consistent linear trend estimates for the dual- and single-accelerometer periods.

The largest difference between our C_{30} solution and those from the original C_{30} during the dual-accelerometer period and those from the SLR data processing is the amplitudes in the seasonal signals. Our results show larger annual amplitude and smaller semiannual amplitude. However, the reasons are still unknown and further investigations are needed in the future.

Another issue is that no matter which C_{30} solution is used, larger annual amplitude estimates are obtained compared to the dual-accelerometer span, which indicates there may be other unidentified problematic coefficients which contribute to an amplification of about 100 Gt for the annual amplitude. Since estimating C_{30} coefficients through the GRACE-OBP approach requires higher degree coefficients as input, such a problem will theoretically increase the uncertainties. Fortunately, these unidentified problematic coefficients are not affecting the estimation of C_{30} significantly as the time series of the two periods are consistent.

Supplementary Information The online version contains supplementary material available at https://doi.org/10.1007/s00190-023-01707-3.

Acknowledgements We thank our editors and three anonymous reviewers for their insightful comments which greatly improved the quality of the manuscript. We thank Riccardo Riva from Delft University of Technology for carefully revising the manuscript as well as constructive suggestions and insightful comments. This study is supported by the National Natural Science Foundation of China (grant 42171426 and 41904009) and open project from Key Lab of Spatial Data Mining and Information Sharing, Ministry of Education (grant 2022LSDMIS06). We estimate AIS mass change time series using a dedicated tool package provided by Wei Feng (Feng 2019). All the figures are prepared by the Generic Mapping Tools (Wessel et al. 2019).

Author Contributions YS and XG conceived the idea and designed all the experiments; YS, YL, and XG performed the research and analyzed the data; YS and XG wrote the paper; JG revised the paper; all authors reviewed and commented on the paper.

Data availability GRACE/GRACE-FO level 2 data are publicly available from the ICGEM website (http://icgem.gfz-potsdam.de/home). The GSFC SLR C_{30} coefficients (TN-14) are taken from https://podaac-tools.jpl.nasa.gov/drive/files/GeodeticsGravity/gracefo/docs/TN-14_C30_C20_GSFC_SLR.txt. The CSR SLR C_{30} coefficients are extracted from http://download.csr.utexas.edu/pub/slr/degree_5/CSR_Monthly_5x5_Gravity_Harmonics.txt. The IGG SLR solution is available at http://icgem.gfz-potsdam.de/series/04_SLR/IGG_SLR_HYBRID. The updated ESM can be accessed at https://isdc.gfz-potsdam.de/esmdata/esaesm/. The A12 GIA model is provided by Geruo A through personal communications. The Caron17 GIA model can be downloaded from https://vesl.jpl.nasa.gov/solid-earth/gia/ and the Peltier18 GIA model can be taken from https://www.atmosp.physics.utoronto.ca/~peltier/data.php. The resulting C_{30} coefficients of this study for CSR, GFZ and JPL GRACE/GRACE-FO level 2 data are available in the supplementary materials. C_{30} time series based on the GRACE-OBP approach using other data center's TVG models are available upon requests.

Declaration

Conflict of interest The authors declare that they have no conflict of interest.

References

A G, Wahr J, Zhong S (2012) Computations of the viscoelastic response of a 3-D compressible Earth to surface loading: an application to Glacial Isostatic Adjustment in Antarctica and Canada. Geophys J Int 192(2):557–572. https://doi.org/10.1093/gji/ggs030

Bandikova T, McCullough C, Kruizinga GL et al (2019) GRACE accelerometer data transplant. Adv Space Res 64(3):623–644. https://doi.org/10.1016/j.asr.2019.05.021

Caron L, Métivier L, Greff-Lefftz M et al (2017) Inverting glacial isostatic adjustment signal using bayesian framework and two linearly relaxing rheologies. Geophys J Int 209(2):1126–1147. https://doi.org/10.1093/gji/ggx083

Chen JL, Wilson CR, Li J et al (2015) Reducing leakage error in GRACE-observed long-term ice mass change: a case study in West Antarctica. J Geodesy 89(9):925–940. https://doi.org/10.1007/s00190-015-0824-2

Cheng M, Ries J (2017) The unexpected signal in GRACE estimates of C_{20}. J Geodesy 91(8):897–914. https://doi.org/10.1007/s00190-016-0995-5

Cheng M, Ries JC, Tapley BD (2011) Variations of the Earth's figure axis from satellite laser ranging and GRACE. J Geophys Res Solid Earth 116(B1):B01409. https://doi.org/10.1029/2010JB000850

Consortium E, Fukumori I, Wang O, et al (2020) Synopsis of the ECCO Central Production Global Ocean and Sea-Ice State Estimate, Version 4 Release 4. Tech. rep., Zenodo, https://doi.org/10.5281/zenodo.3765929

Dee DP, Uppala SM, Simmons AJ et al (2011) The ERA-Interim reanalysis: configuration and performance of the data assimilation system. Q J R Meteorol Soc 137(656):553–597. https://doi.org/10.1002/qj.828

Devoti R, Luceri V, Sciarretta C et al (2001) The SLR secular gravity variations and their impact on the inference of mantle rheology and lithospheric thickness. Geophys Res Lett 28(5):855–858. https://doi.org/10.1029/2000GL011566

Ditmar P, Tangdamrongsub N, Ran J et al (2018) Estimation and reduction of random noise in mass anomaly time-series from satellite gravity data by minimization of month-to-month year-to-year double differences. J Geodyn 119:9–22. https://doi.org/10.1016/j.jog.2018.05.003

Dobslaw H, Bergmann-Wolf I, Dill R et al (2015) The updated ESA earth system model for future gravity mission simulation studies. J Geodesy 89(5):505–513. https://doi.org/10.1007/s00190-014-0787-8

Duan XJ, Guo JY, Shum CK et al (2009) On the postprocessing removal of correlated errors in GRACE temporal gravity field solutions. J Geodesy 83(11):1095–1106. https://doi.org/10.1007/s00190-009-0327-0

Feng W (2019) GRAMAT: a comprehensive Matlab toolbox for estimating global mass variations from GRACE satellite data. Earth Sci Inf 12(3):389–404. https://doi.org/10.1007/s12145-018-0368-0

Gruber T, Bamber JL, Bierkens MFP et al (2011) Simulation of the time-variable gravity field by means of coupled geophysical models. Earth Syst Sci Data 3(1):19–35. https://doi.org/10.5194/essd-3-19-2011

Jeon T, Seo KW, Youm K et al (2018) Global sea level change signatures observed by GRACE satellite gravimetry. Sci Rep 8(1):1–10. https://doi.org/10.1038/s41598-018-31972-8

Jungclaus JH, Fischer N, Haak H et al (2013) Characteristics of the ocean simulations in the max planck institute ocean model (MPIOM) the ocean component of the MPI-earth system model. J Adv Model Earth Syst 5(2):422–446. https://doi.org/10.1002/jame.20023

Kusche J, Schmidt R, Petrovic S et al (2009) Decorrelated GRACE time-variable gravity solutions by GFZ, and their validation using a hydrological model. J Geodesy 83(10):903–913. https://doi.org/10.1007/s00190-009-0308-3

Landerer FW, Flechtner FM, Save H et al (2020) Extending the global mass change data record: grace follow-on instrument and science data performance. Geophys Res Lett 47(12):e2020GL088306. https://doi.org/10.1029/2020GL088306

Loomis BD, Rachlin KE, Wiese DN et al (2020) Replacing GRACE/GRACE-FO C_{30} with satellite laser ranging: impacts on antarctic ice sheet mass change. Geophys Res Lett 47(3):e2019GL085488. https://doi.org/10.1029/2019GL085488

Löcher A, Kusche J (2020) A hybrid approach for recovering high-resolution temporal gravity fields from satellite laser ranging. J Geodesy 95(1):6. https://doi.org/10.1007/s00190-020-01460-x

Marshall J, Adcroft A, Hill C et al (1997) A finite-volume, incompressible navier stokes model for studies of the ocean on parallel computers. J Geophys Res Ocean 102(C3):5753–5766. https://doi.org/10.1029/96JC02775

Peltier WR, Argus DF, Drummond R (2018) Comment on "An Assessment of the ICE-6G_C (VM5a) Glacial Isostatic Adjustment Model" by Purcell. J Geophys Res Solid Earth 123(2):2019–2028. https://doi.org/10.1002/2016JB013844

Seo KW, Kim JS, Youm K et al (2021) Secular polar motion observed by GRACE. J Geodesy 95(4):40. https://doi.org/10.1007/s00190-021-01476-x

Sośnica K, Jäggi A, Meyer U et al (2015) Time variable Earth's gravity field from SLR satellites. J Geodesy 89(10):945–960. https://doi.org/10.1007/s00190-015-0825-1

Sun Y, Ditmar P, Riva R (2016) Observed changes in the Earth's dynamic oblateness from GRACE data and geophysical models. J Geodesy 90(1):81–89. https://doi.org/10.1007/s00190-015-0852-y

Sun Y, Riva R, Ditmar P (2016) Optimizing estimates of annual variations and trends in geocenter motion and J_2 from a combination of GRACE data and geophysical models. J Geophys Res Solid Earth 121(11):8352–8370. https://doi.org/10.1002/2016JB013073

Sun Y, Ditmar P, Riva R (2017) Statistically optimal estimation of degree-1 and C_{20} coefficients based on GRACE data and an ocean bottom pressure model. Geophys J Int 210(3):1305–1322. https://doi.org/10.1093/gji/ggx241

Sun Y, Riva R, Ditmar P et al (2019) Using GRACE to explain variations in the earth's oblateness. Geophys Res Lett 46(1):158–168. https://doi.org/10.1029/2018GL080607

Swenson S, Wahr J (2006) Post-processing removal of correlated errors in GRACE data. Geophys Res Lett 33(8):L08402. https://doi.org/10.1029/2005GL025285

Swenson S, Chambers D, Wahr J (2008) Estimating geocenter variations from a combination of GRACE and ocean model output. J Geophys Res Solid Earth 113(B8):B08410. https://doi.org/10.1029/2007JB005338

Tapley BD, Bettadpur S, Watkins M et al (2004) The gravity recovery and climate experiment: mission overview and early results. Geophys Res Lett 31(9):L09607. https://doi.org/10.1029/2004GL019920

Tapley BD, Watkins MM, Flechtner F et al (2019) Contributions of GRACE to understanding climate change. Nat Clim Chang 9(5):358. https://doi.org/10.1038/s41558-019-0456-2

Wahr J, Molenaar M, Bryan F (1998) Time variability of the Earth's gravity field: hydrological and oceanic effects and their possible detection using GRACE. J Geophys Res Solid Earth 103(B12):30205–30229. https://doi.org/10.1029/98JB02844

Wessel P, Luis JF, Uieda L et al (2019) The generic mapping tools version 6. Geochem Geophys Geosyst 20(11):5556–5564. https://doi.org/10.1029/2019GC008515

Wiese DN, Nerem RS, Han SC (2011) Expected improvements in determining continental hydrology ice mass variations ocean bottom pressure signals and earthquakes using two pairs of dedicated satellites for temporal gravity recovery. J Geophys Res Solid Earth. https://doi.org/10.1029/2011JB008375

Wu X, Ray J, van Dam T (2012) Geocenter motion and its geodetic and geophysical implications. J Geodyn 58:44–61. https://doi.org/10.1016/j.jog.2012.01.007